Petroleum Research 11 (2026) 237–249

Contents lists available at ScienceDirect

Petroleum Research

journal homepage: http://www.keaipublishing.com/en/journals/petroleum-research/

Full Length Article

Study on the expansion characteristics of oil-based drilling fluid in HTHP wellbore

Mingjie Cai *, Dan Mao, Yuyao Li, Tingjun He, Mingmin He, Leichuan Tan

CNPC Chuanqing Drilling Engineering Company Limited, Chengdu, Sichuan, 610000, China

ARTICLE INFO

Article history:
Received 3 March 2025
Received in revised form
3 August 2025
Accepted 3 August 2025
Available online 7 August 2025

Keywords:
Oil-based drilling fluid
Expansion characteristics
HTHP well
Temperature prediction

ABSTRACT

Accurate prediction of oil-based drilling fluid (OBD) behavior under high-temperature, high-pressure (HTHP) conditions in ultra-deep wells is essential for ensuring well control safety. However, research on the volumetric expansion of OBD in HTHP wellbores remains limited. This study develops a mathematical model to predict the expansion characteristics of OBD in HTHP wellbores, incorporating temperature- and pressure-dependent variations in rheological properties, thermophysical parameters, and density. The model is solved using discretization and the successive over-relaxation (SOR) method. Laboratory experiments were conducted to measure the rheology and density of OBD at different initial densities under varying temperature and pressure conditions. Binary mathematical models describing density and rheology as functions of temperature and pressure were established. The results indicate that the rheological properties of OBD exhibit consistent trends across different initial densities. Apparent viscosity (AV) and plastic viscosity (PV) decrease with increasing temperature and gradually stabilize, while both increase with rising pressure. The density of OBD decreases due to thermal expansion at elevated temperatures and increases due to thermal contraction at lower temperatures. Temperature exerts a greater effect on OBD density than pressure. Model validation using field data from an ultra-deep well confirms the accuracy of the proposed approach. During drilling and tripping operations, changes in mud pit volume occur due to temperature fluctuations; however, these changes are relatively slow compared to the rapid volume changes associated with wellbore influx. It is recommended to suspend the use of drilling fluid cooling devices before pulling out of hole (POOH) operations to minimize mud pit volume fluctuations. These findings provide theoretical guidance for accurate bottom-hole temperature prediction and improved drilling strategy optimization.

© 2025 Chinese Petroleum Society. Publishing services by Elsevier B.V. on behalf of KeAi Communications Co. Ltd. This is an open access article under the CC BY-NC-ND license (http://creativecommons.org/licenses/by-nc-nd/4.0/).

1. Introduction

With the global shortage of oil and gas resources intensifying, drilling operations have progressively shifted to deep and ultra-deep reservoirs (Ding et al., 2023; Zhou et al., 2025). Oil-based drilling fluid (OBD) is widely used in ultra-deep drilling due to its salt and calcium invasion resistance, favorable lubricity, minimal water loss, and low formation damage (James et al., 2000; Malachosky et al., 1991). However, in high-temperature and high-pressure (HTHP) wells, the properties of OBDs are not stable, leading to changes in rheological behavior, density, and thermophysical parameters (Zhong et al., 2019; Mahmoud et al., 2025). Such changes affect bottom-hole pressure, increasing the risk of overflow, and alter the drilling fluid volume in the wellbore, thereby changing the total drilling fluid volume (Kabir et al., 1996). These effects ultimately increase well control risks and add uncertainty to ultra-deep drilling. Therefore, accurately predicting the characteristics of drilling fluids under HTHP conditions is essential to reduce drilling risk.

Numerous researchers have investigated changes in the physical properties of OBD under HTHP conditions using experimental and theoretical approaches. Their work has clarified the variations in rheological behavior and density of OBDs with temperature and pressure (Xie et al., 2021; Mcmordie et al., 1982; Jiang et al., 2022; Zhao et al., 2009). Some predictive models have accounted for the influence of rheology on the drilling temperature field. For example, Liu et al. (2024) developed a temperature–pressure coupling model that considers variations in fluid properties, and proposed a segmented prediction method for fluid density and rheology. Yu et al. (2021) established a model to predict wellbore

* Corresponding author.
E-mail address: caimj1994@qq.com (M. Cai).
Peer review under the responsibility of Editorial Office of Petroleum Research.

https://doi.org/10.1016/j.ptlrs.2025.08.003
2096-2495/© 2025 Chinese Petroleum Society. Publishing services by Elsevier B.V. on behalf of KeAi Communications Co. Ltd. This is an open access article under the CC BY-NC-ND license (http://creativecommons.org/licenses/by-nc-nd/4.0/).

temperature and pressure during drilling in Arctic regions, incorporating the association between permafrost and wellbore, and the effects of low temperature on OBD rheology. In addition, the wellbore temperature field has also been widely studied. Wang et al. established a temperature and pressure coupled downhole heat transfer model to analyze how fourteen factors affect wellbore temperature. The influencing factors that can be used to guide the drilling fluid's cooling technology were drilling fluid thermal conductivity, drilling fluid heat capacity, drilling fluid density, drill strings rotation speed, pump rate, viscosity, ROP, and injection temperature (Wang et al., 2024). Xiao et al. (2024) proposed a coupling model of wellbore heat transfer and cuttings bed height to study the influences of the circulation time, circulation flow rate, drill pipe rotation speed, rate of penetration, and inlet temperature on the wellbore heat transfer. Measures to reduce the downhole temperature were proposed. Mao et al. (2024) established a transient heat transfer model for geothermal horizontal wells with heat–fluid–solid coupling, they analyzed the effects of the drilling fluid system, density, and displacement, rotary speed, and WOB during drilling on the wellbore temperature distribution. It is noticed that, beyond rheology, the thermophysical properties and density of OBDs are also affected by temperature and pressure changes. Currently, no temperature field model simultaneously couples the variations in OBD rheology, density, and thermophysical properties under high temperature and pressure. Furthermore, changes in OBD volume in the wellbore resulting from temperature and pressure fluctuations have not been previously addressed.

Therefore, this work establishes a mathematical model to predict OBD expansion in the HTHP wellbore. The model incorporates the effects of temperature and pressure on the rheological behavior, thermophysical parameters, and density of OBD. The relationships between density, rheology, and temperature/pressure are determined experimentally and through fitting, whereas thermophysical parameters as a function of temperature and pressure are obtained from the literature. Model validation is performed by inverting field data from an ultra-deep well.

2. Mathematical model of OBD HTHP expansion

Accurate prediction of the volume change of OBD under HTHP conditions requires determination of the wellbore temperature and pressure distribution. The distributions of downhole pressure and temperature differ under various operational conditions, as illustrated in Fig. 1. The pressure distribution model under normal drilling and tripping (trip) conditions can be expressed as follows:

$$P(h,t)=\begin{cases}\rho_o(P,T)\cdot g\cdot h+P_f(Circulation)\\ \rho_o(P,T)\cdot g\cdot h-P_w(POOH)\\ \rho_o(P,T)\cdot g\cdot h+P_g(RIH)\end{cases} \quad (1)$$

where, $\rho_o(P,T)$ is the density of OBD, which changes with pressure and temperature; h is the well depth; P_f is the circulating pressure loss; P_w is the swab pressure during pull out of hole (POOH); P_g is the surge pressure during run in hole (RIH).

As depicted in Fig. 1, during drilling, the pump system circulates drilling fluid from the circulation tank through the riser and drilling hose into the drill pipe. The fluid travels downward inside the drill string and returns upward along the annulus, located between the wellbore and the drill string, after exiting the bit nozzle. Upon returning to the wellhead, the fluid re-enters the circulation tank. This circulation process generates heat through friction between the drilling fluid and the borehole wall (either formation or casing). In addition, convective heat transfer occurs due to

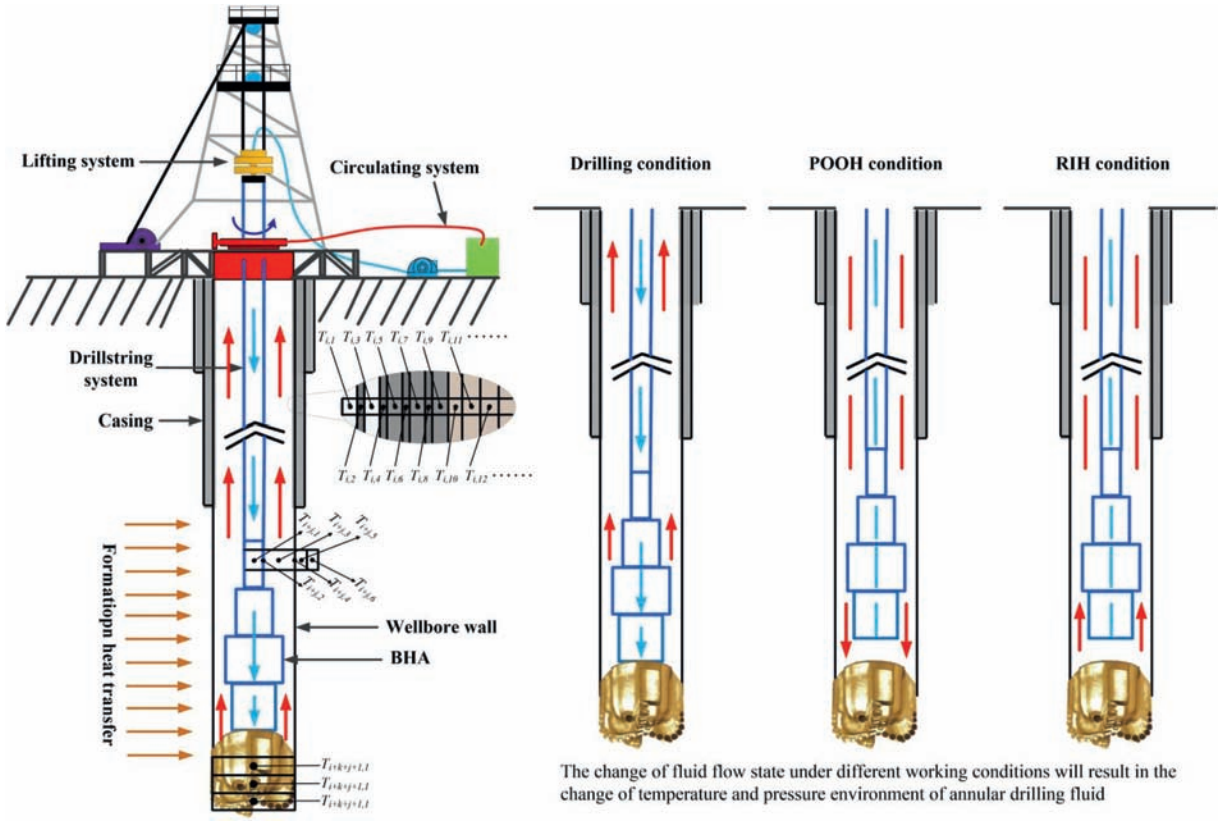


Fig. 1. Physical model of drilling system under different working conditions.

temperature differences between fluids. Heat from the formation is transferred to the near-wellbore region via thermal conduction, with further convective heat transfer occurring between the drilling fluid, the wellbore, and the drill pipe. Friction between the drill bit and the rock during rock breaking also contributes to temperature variation in the drilling fluid. Therefore, the annular drilling fluid temperature distribution is affected by the operational condition, and differences in annular temperature fields under drilling and trip conditions cause changes in drilling fluid properties. Therefore, it is essential to establish a coupled pressure and temperature prediction model for different working conditions.

The heat transfer system comprises the drilling fluid, drill string, annulus, wellbore wall, cement, and formation, with both thermal conduction and convection processes present. For modeling, a control volume P is defined, with boundaries labeled e, s, w, and n (east, south, west, and north, respectively). The adjacent control volumes in these directions are designated as E, S, W, and N. The relationship between control volume P and its adjacent volumes is shown in Fig. 2. The corresponding energy balance is given by.

$$U_P^1 - U_P^0 = Q_n^{0-1} - Q_s^{0-1} + Q_e^{0-1} + S_p^{0-1} \tag{2}$$

Based on the principle of energy conservation, heat transfer models are developed for each component: the fluid inside the drill string, the drill string itself, the annular fluid, and the formation. The detailed derivation is provided in Appendix A.

(1) Drilling Fluid Inside the Drill String

$$\begin{aligned}\pi r_1^2 \Delta z\left[(\overline{c\rho T})_P^1 - (\overline{c\rho T})_P^0\right] &= \pi r_1^2 \Delta t\left[(\overline{c\rho v_i T})_n^{0-1} - (\overline{c\rho v_i T})_s^{0-1}\right] \\ &+ 2\pi r_1 \Delta z \Delta t[\overline{k_e(T_E - T_P)}]^{0-1} \\ &+ \frac{1}{4}\pi r_1 f_s \Delta z \Delta t\left(\overline{\rho v_i^3}\right)^{0-1}\end{aligned} \tag{3}$$

(2) Heat Transfer Model for Drill String and Drill Bit

For control volumes representing the drill string, frictional heat generation Q_{pf} between the drill string and the wellbore wall appears on the right side of the equation, mathematically expressed as:

$$\begin{aligned}\pi\left(r_2^2 - r_1^2\right)\Delta z c_P \rho_P\left(T_P^1 - T_P^0\right) &= \pi\left(r_2^2 - r_1^2\right)\Delta t[\overline{k_P(T_S + T_N - 2T_P)}]^{0-1} \\ &+ 2\pi\Delta z\Delta t\Big\{r_2[\overline{k_e(T_E - T_P)}]^{0-1} \\ &- r_1\left[\overline{k_w(T_p - T_W)}\right]^{0-1}\Big\} + Q_{pf}\end{aligned} \tag{4}$$

For the drill bit, frictional heat Q_{rg} generated between the bit and the formation is similarly included:

$$\begin{aligned}\pi\left(r_2^2 - r_1^2\right)\Delta z c_P \rho_P\left(T_P^1 - T_P^0\right) &= \pi\left(r_2^2 - r_1^2\right)\Delta t[\overline{k_P(T_P - T_N)}]^{0-1} \\ &+ 2\pi\Delta z\Delta t\Big\{r_2[\overline{k_e(T_E - T_P)}]^{0-1} \\ &- r_1\left[\overline{k_w(T_p - T_W)}\right]^{0-1}\Big\} + Q_{rg}\end{aligned} \tag{5}$$

Friction during drilling is dynamic, resulting in spatial and temporal fluctuations in contact forces and frictional heat generation. In this work, frictional heat Q_{pf} between the drill string and the wellbore wall is calculated using the dynamic drillstring model established in the authors' previous work (Cai et al., 2022).

(3) Annular Drilling Fluid

$$\begin{aligned}\pi\left(r_3^2 - r_2^2\right)\Delta z\left[(\overline{c\rho T})_P^1 - (\overline{c\rho T})_P^0\right] &= \pi\left(r_3^2 - r_2^2\right)\Delta t\left[(\overline{c\rho v_a T})_s^{0-1}\right. \\ &\left. - (\overline{c\rho v_a T})_n^{0-1}\right] \\ &+ 2\pi\Delta z\Delta t\Big\{r_3[\overline{k_e(T_E - T_P)}]^{0-1} \\ &- r_2[\overline{k_w(T_P - T_W)}]^{0-1}\Big\} \\ &+ \frac{1}{4}\pi(r_2 + r_3) f_s \Delta z \Delta t\left(\overline{\rho v_a^3}\right)^{0-1}\end{aligned} \tag{6}$$

(4) Near-Wellbore Formation

The energy equation for the formation near the wellbore is expanded as:

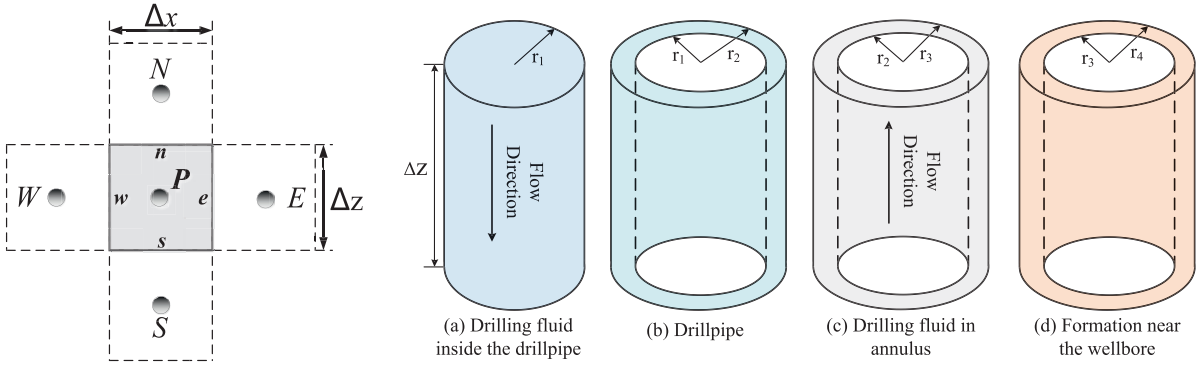


Fig. 2. Diagrams of control body.

$$\pi\left(r_4^2-r_3^2\right)\Delta z c_P\rho_P\left(T_P^1-T_P^0\right)=\pi\left(r_4^2-r_3^2\right)\Delta t[\overline{k_P(T_S+T_N-2T_P)}]^{0-1}+2\pi\Delta z\Delta t\left\{r_4[\overline{k_e(T_E-T_P)}]^{0-1}-r_3\left[\overline{k_w(T_p-T_W)}\right]^{0-1}\right\} \tag{7}$$

where the subscript P represents the current control volume, and E, S, W, and N denote the four adjacent volumes. The superscript 0 refers to the current time step and 1 to the subsequent time step.

The temperature model is solved via discretization and the Successive Over-Relaxation (SOR) method, as detailed in Appendix B. The coupled pressure and temperature prediction model can then be computed following the procedure shown in Fig. 3. For the OBD system, rheological properties, thermophysical parameters, and density change with temperature and pressure (Santoyo et al., 2001). It is necessary to update the fluid properties according to pressure and temperature variations to accurately characterize the wellbore temperature and pressure distribution. Thus, the relationships governing OBD rheological property, thermophysical parameters, and density as functions of temperature and pressure must be established. The expansion volume of a unit volume of OBD due to temperature variation is determined according to the law of mass conservation:

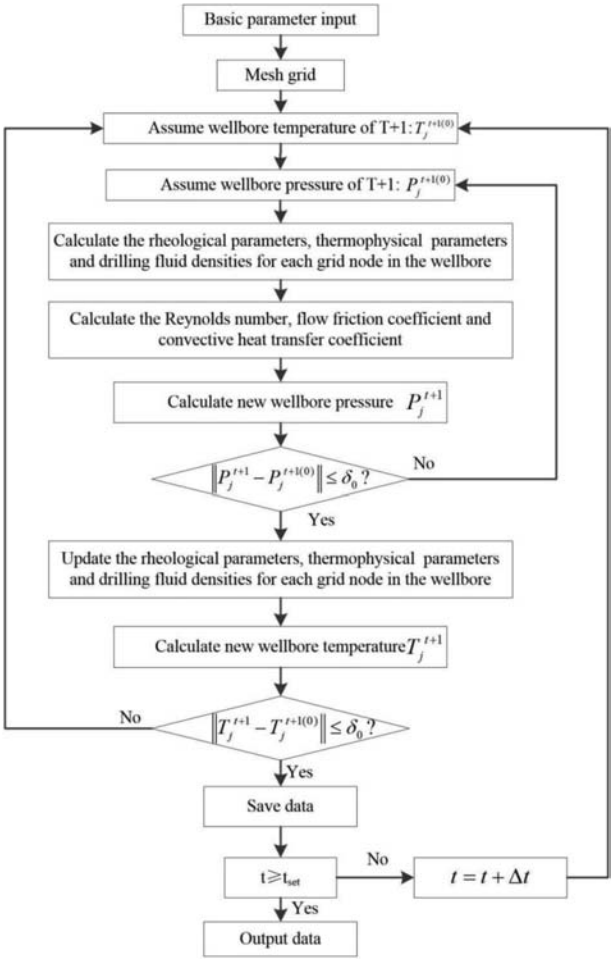


Fig. 3. Calculation flow of the coupled model.

$$\Delta V(P,T)=\left(\frac{\rho_1}{\rho_2(P,T)}-1\right)\cdot V_0 \tag{8}$$

Thus, the total OBD expansion in a given period of time can be calculated by the equation:

$$V_t=\sum_0^H\Delta V(P,T) \tag{9}$$

3. Determination of OBD properties under HTHP conditions

The sensitivity of OBD to temperature and pressure varies due to different interactions between components under different density conditions (Fan et al., 2024). Therefore, experimental studies were conducted under different density conditions. Four OBD densities were selected to evaluate the temperature and pressure sensitivity of rheological properties and density. The drilling fluid materials were supplied by Chuanqing Drilling Engineering Co., Ltd., and their detailed compositions are listed in Table 1. Fig. 4 presents the experimental instruments used, including the HTHP rheology tester IX77 (Fann, USA) and the liquid HTHP density meter. The HTHP rheometer operates at maximum conditions of 310 °C and 200 MPa, while the liquid HTHP density meter operates at up to 300 °C and 120 MPa.

3.1. HTHP rheological property

Fig. 5 shows the 3D cloud diagrams of the rheological test results for OBD at different densities. The trends in rheological properties are consistent across densities. Specifically, the apparent viscosity (AV) and plastic viscosity (PV) of OBD decrease with increasing temperature and tend to stabilize, while both increase with increasing pressure. Based on the experimental results, mathematical analyses were performed to derive binary rheological models for AV, PV, and yield point (YP) using temperature and pressure as independent variables, expressed as:

$$\begin{cases}\mu_{AV}=\mu_{0AV}\exp\left(\alpha_{1AV}*(T-T_0)^2+\alpha_{2AV}*(T-T_0)+\alpha_{3AV}*(P-P_0)\right.\\ \mu_{PV}=\mu_{0PV}\exp\left(\alpha_{1PV}*(T-T_0)^2+\alpha_{2PV}*(T-T_0)+\alpha_{3PV}*(P-P_0)\right.\\ \mu_{YP}=\mu_{AV}-\mu_{PV}\end{cases} \tag{10}$$

where, μ_{0AV} and μ_{0PV} represent the apparent viscosity and plastic viscosity at 65 °C and 0.1 MPa; P represents the pressure condition of the OBD; T represents the temperature condition of the OBD; μ_{YP} is the yield point of OBD; α_1、 α_2、 α_3 are the fitting coefficients, provided in Table 2.

3.2. HTHP density

Fig. 6 presents the 3D cloud diagrams of density test results for OBD at different initial densities. The results indicate that the density decreases due to thermal expansion at high temperatures and increases due to contraction at lower temperatures. Under high pressure, density increases due to internal compaction, whereas it decreases under lower pressure conditions. Comparison shows that temperature has a greater effect on OBD density than pressure. This is primarily due to the high solid content and poor compressibility of the solid–liquid dispersion system of drilling fluid. Furthermore, increases in density are accompanied

Table 1
Detailed compositions and initial performance of OBD.

Density	Composition	Initial AV (65 °C + 0.1 MPa)	Initial PV (65 °C + 0.1 MPa)	Initial density (65 °C + 0.1 MPa)
2.40 g/cm^3	170 mL diesel+5.5% emulgator+1%wetting agent+30mLsaline+4%oxidized asphalt+2% sealing agent+5%calcium oxide+(220gMn3O4+480gbarite)	66 mPa s	60 mPa s	2.40 g/cm^3
2.20 g/cm^3	170 mL diesel+5.5% emulgator+1%wetting agent+30mLsaline+4%oxidized asphalt+2% sealing agent+5%calcium oxide+(200gMn3O4+450gbarite)	64 mPa s	59 mPa s	2.20 g/cm^3
1.80 g/cm^3	170 mL diesel+8% emulgator+1%wetting agent+30mLsaline+4%oxidized asphalt+2% sealing agent+5%calcium oxide+(100gMn3O4+250gbarite)	30 mPa s	27 mPa s	1.80 g/cm^3
1.40 g/cm^3	160 mL diesel+9% emulgator+1%wetting agent+35mLsaline+4%oxidized asphalt+2% sealing agent+5%calcium oxide+3% organic soil+ (80gMn3O4+180gbarite)	23 mPa s	21 mPa s	1.40 g/cm^3

by greater internal friction within the treatment agents in the drilling fluid, which increases both viscosity and shear force. The experimental data were further analyzed mathematically, and a binary density model was established with temperature and pressure as independent variables, as follows:

$$\rho = \rho_0 + \beta_0 * P + \beta_1 * T + \beta_2 * P * T + \beta_3 * T_2 + \beta_4 * T_3 \tag{11}$$

where, ρ_0 represents the density of OBD at 0 °C under vacuum conditions; $\beta_0, \beta_1, \beta_2, \beta_3, \beta_4$ are fitting coefficients, listed in Table 3. The fitting coefficients across different densities show similar magnitudes and no clear trend with changing density. Furthermore, the coefficients of determination (R^2) exceed 0.97 for all densities, demonstrating that the regression models accurately describe the observed variations.

3.3. HTHP thermophysics property

Thermophysical properties are experimentally confirmed to be strongly affected by temperature and drilling fluid density. In this study, the empirical fitting equations proposed by Mao et al. (2023) were applied to quantify the influence of temperature on the thermophysical properties of the drilling fluid:

$$\begin{cases} k = 0.00032524T + 0.29173\rho - 0.14316 \\ c = 3.202T - 589.9\rho + 1870.6 \end{cases} \tag{12}$$

4. Field verification

Well A is an ultra-deep well drilled using OBD to a depth of 8000 m. The well structure of Well A is presented in Fig. 7. The drill bit diameter is 323.585 mm, and combined drill pipes of 139.7 mm and 149.2 mm are utilized. The initial drilling fluid density is 1.77 kg/m3, the plastic viscosity is 42 mPa s, and the dynamic shear force is 5.5 Pa. To decrease the downhole temperature and extend the service life of the drilling tools, a surface circulation cooling device is employed during drilling. This device lowers the outlet drilling fluid temperature by approximately 15 °C and the inlet drilling fluid temperature by about 25 °C. When the cooling device fails or a tripping operation is performed, the wellbore temperature distribution changes, which affects both the density and volume of the OBD in the wellbore and results in drilling fluid expansion or contraction.

Fig. 8 shows the measured variation in total pit gain, outlet temperature, and inlet temperature when the cooling device ceases operation. When the cooling device stops, the inlet tem-

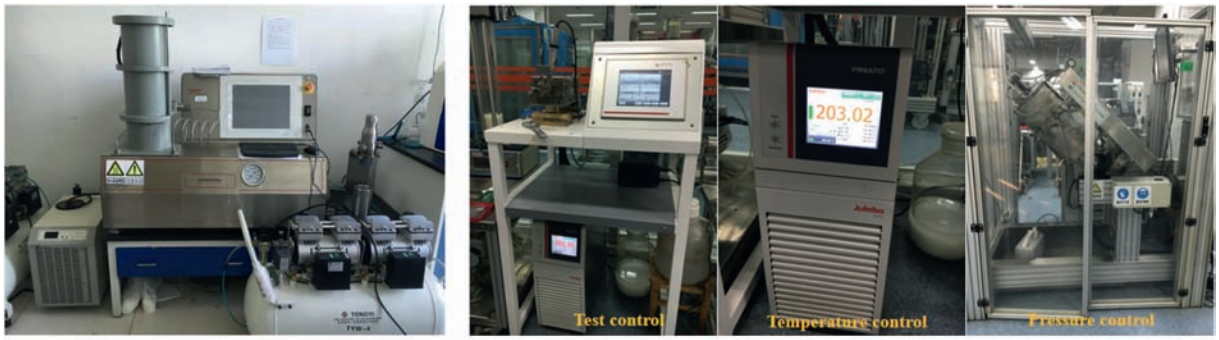


Fig. 4. Experimental apparatus.

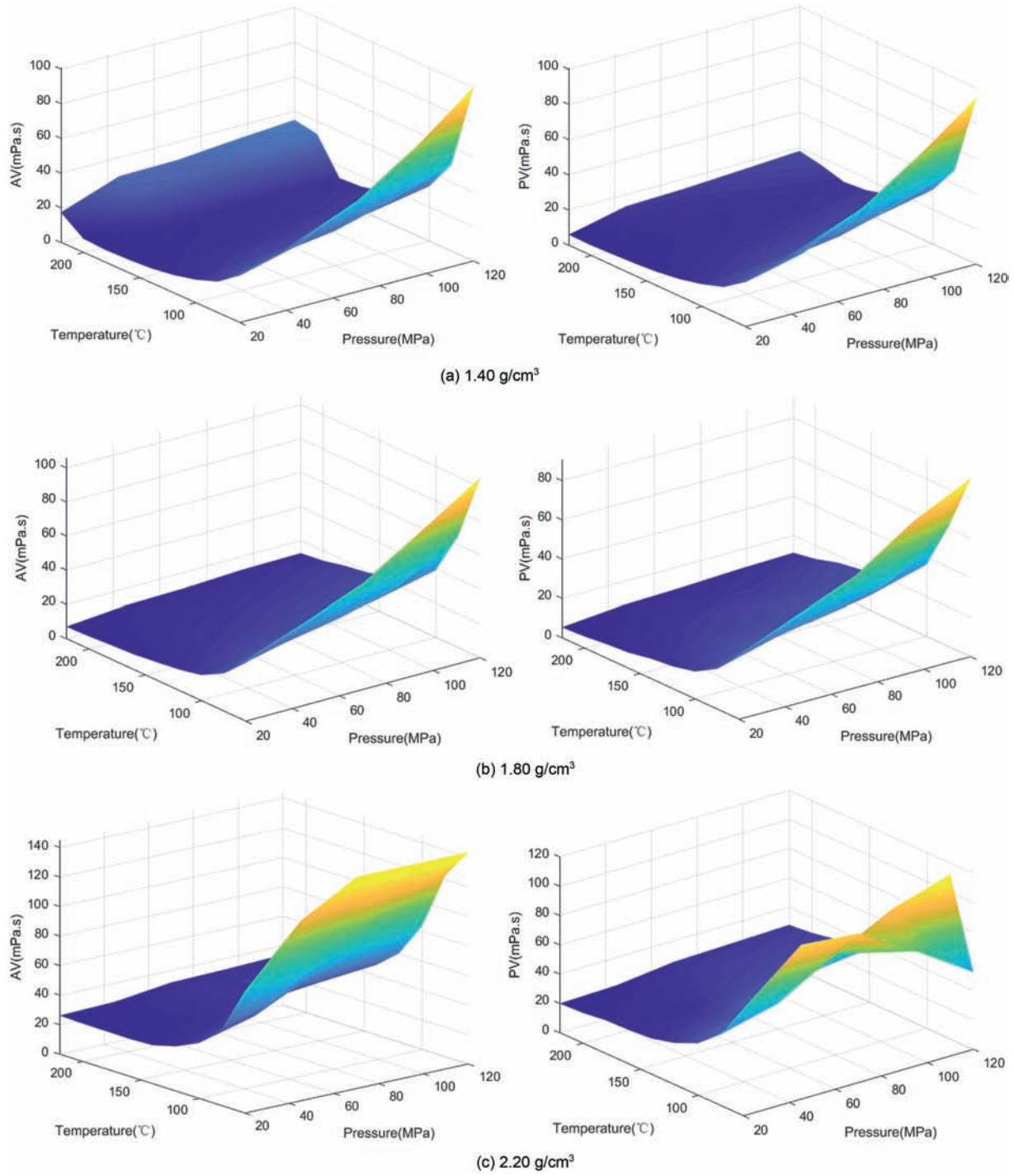


Fig. 5. 3D cloud diagrams of rheological test results for OBD at different densities.

perature increases from 43 °C to 67 °C, and the outlet temperature increases from 57 °C to 69 °C. Concurrently, the mud pit volume exhibits a gradual increase, with a cumulative rise of 3.4 m^3 OBD over 20,000 s. The established model in this study is applied to evaluate this phenomenon. Fig. 9 presents the annular temperature and density distributions with and without the cooling device. As shown in Fig. 9a, the outlet temperature increases from 56 °C to 71 °C, closely matching the measured data. The trend of

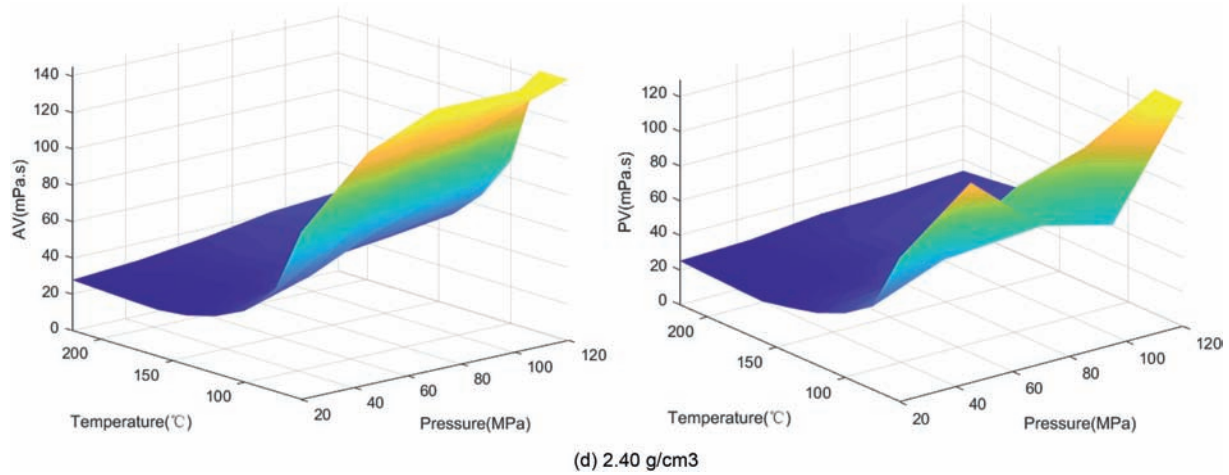


Fig. 5. (*continued*).

Table 2
Fitting coefficients of rheological mathematical models.

Density(g/cm^3)	Viscosity(mPa.s)	α_1	α_2	α_3	R
2.4	AV	$9.72*10^{-5}$	$-2.348*10^{-2}$	$9.086*10^{-3}$	0.98
	PV	$8.703*10^{-5}$	$-2.254*10^{-2}$	$9.243*10^{-3}$	0.97
2.2	AV	$8.82*10^{-5}$	$-2.251*10^{-2}$	$8.532*10^{-3}$	0.96
	PV	$7.177*10^{-5}$	$-2.075*10^{-2}$	$8.21*10^{-3}$	0.98
1.8	AV	$9.483*10^{-5}$	$-2.529*10^{-2}$	$9.328*10^{-3}$	0.99
	PV	$8.188*10^{-5}$	$-2.358*10^{-2}$	$9.132*10^{-3}$	0.99
1.4	AV	$1.471*10^{-4}$	$-3.085*10^{-2}$	$1.042*10^{-2}$	0.98
	PV	$1.402*10^{-4}$	$-3.032*10^{-2}$	$1.063*10^{-2}$	0.98

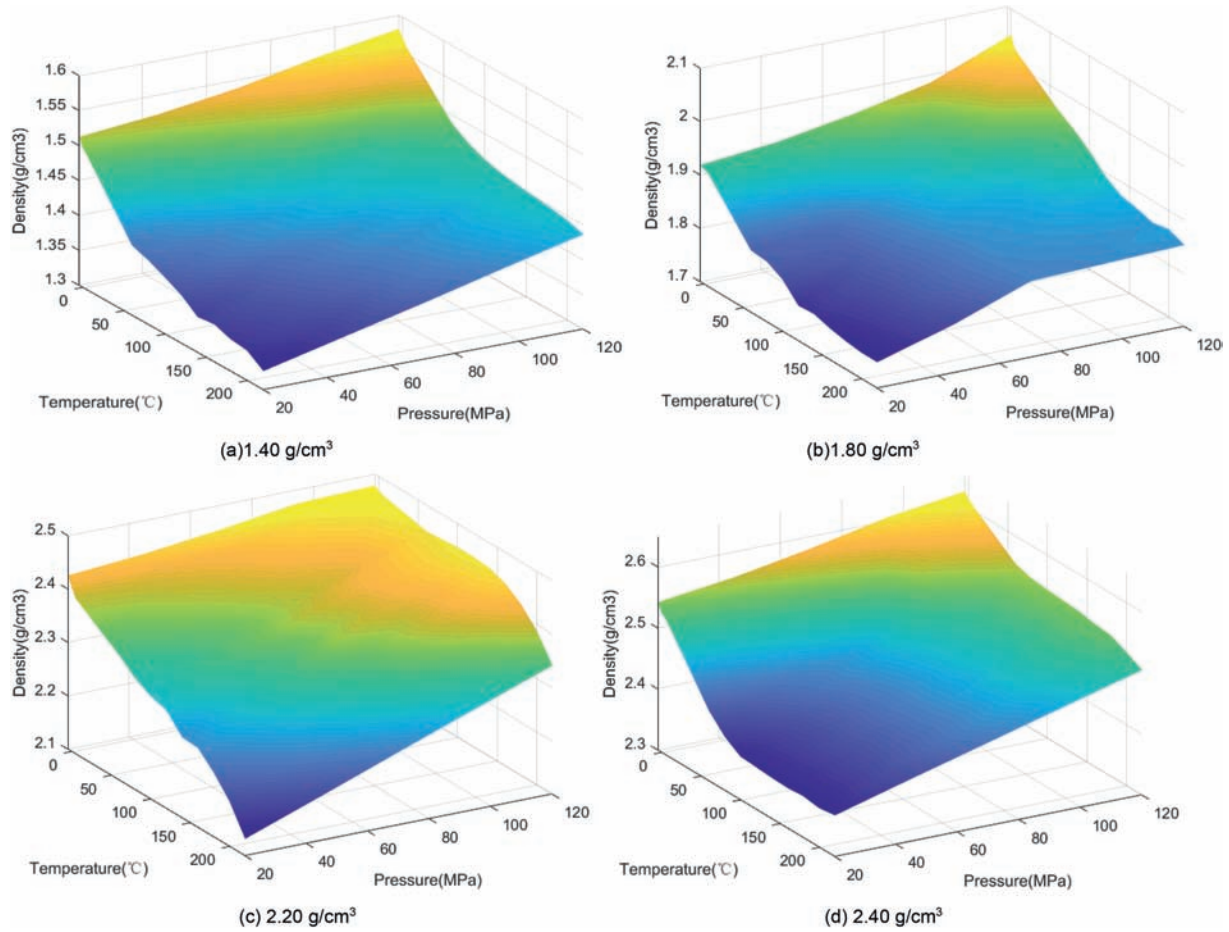


Fig. 6. 3D cloud image of density test results of OBD at different initial densities.

Table 3
Fitting coefficients of density mathematical models.

Density(g/cm^3)	ρ_0	β_0	β_1	β_2	β_3	β_4	R^2
2.4	2.50	$1.078*10^{-3}$	$-2.488*10^{-3}$	$3.163*10^{-6}$	$1.461*10^{-5}$	$-3.255*10^{-8}$	0.99
2.2	2.36	$8.374*10^{-4}$	$-1.976*10^{-3}$	$6.493*10^{-6}$	$1.418*10^{-5}$	$-5.198*10^{-8}$	0.99
1.8	1.87	$1.309*10^{-3}$	$-1.632*10^{-3}$	$-1.053*10^{-6}$	$7.169*10^{-6}$	$1.093*10^{-8}$	0.97
1.4	1.48	$6.87*10^{-4}$	$-2.149*10^{-3}$	$1.76*10^{-6}$	$1.129*10^{-5}$	$-2.383*10^{-8}$	0.99

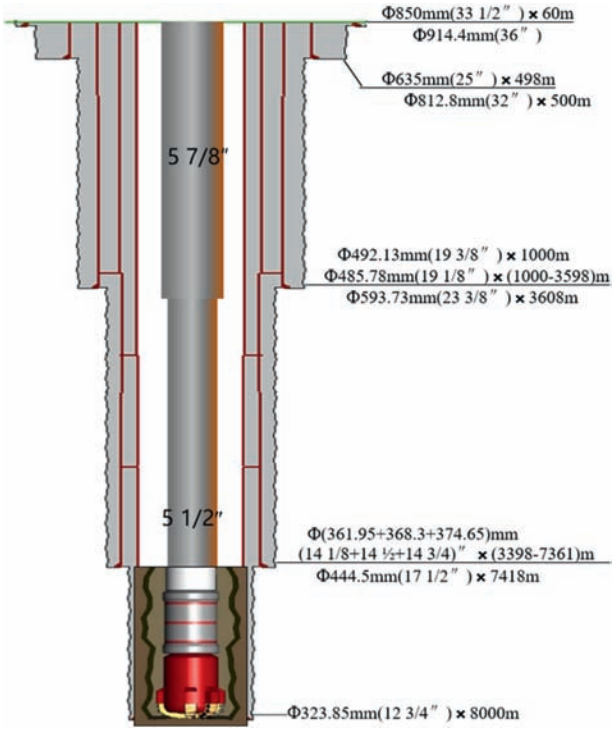


Fig. 7. Well structure of Well A.

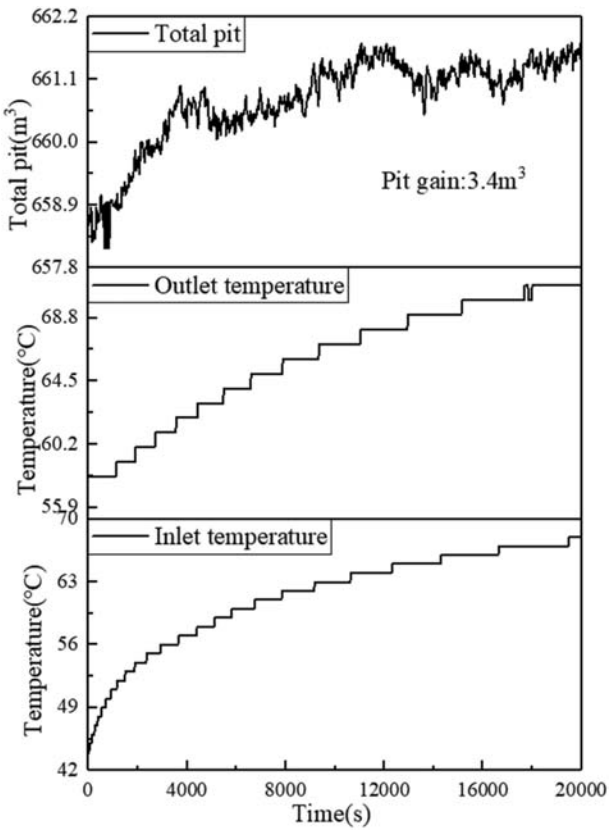


Fig. 8. Measured variation of total pit gain, outlet temperature, and inlet temperature when the cooling device stops.

OBD density is opposite to that of temperature; higher temperatures correspond to lower OBD densities (Fig. 9b), which also indicates that temperature has a greater effect on OBD than pressure. Fig. 10 illustrates the expansion volume distribution along the wellbore depth. The OBD expands at all positions along the wellbore as temperature increases. The predicted total pit gain is 3.28 m^3, which aligns closely with the measured value.

Fig. 11 presents the measured pit gain variation during POOH and RIH conditions. During the POOH process, when the drilling tool is removed from the wellbore, the drilling fluid level decreases. To balance formation pressure, drilling fluid must be continuously pumped into the wellbore, and the volume of fluid pumped should equal the volume of the drilling tool removed. During RIH, as the drilling tool enters the wellbore, drilling fluid is displaced out, and the returned fluid volume should equal the volume of the tool entering the well. As shown in Fig. 11a, during POOH, the actual pumped fluid volume exceeds the theoretical value, indicating a reduction in the wellbore drilling fluid volume. Moreover, as the length of drilling tool removed increases (after 5000 m), the reduction in drilling fluid volume decreases. During RIH, the volume of returned drilling fluid decreases as RIH depth increases. When the RIH depth reaches 4000 m, the returned fluid volume is approximately equal to the theoretical value, as shown in Fig. 11b.

The established model explains this phenomenon well. As illustrated in Fig. 12a, after stopping the pump, the annular drilling fluid temperature above 5800 m exceeds the formation temperature, resulting in heat transfer from the fluid to the formation, which lowers fluid temperature, reduces volume, and increases density. Below 5800 m, the drilling fluid temperature is lower than the formation temperature, resulting in heat transfer from the

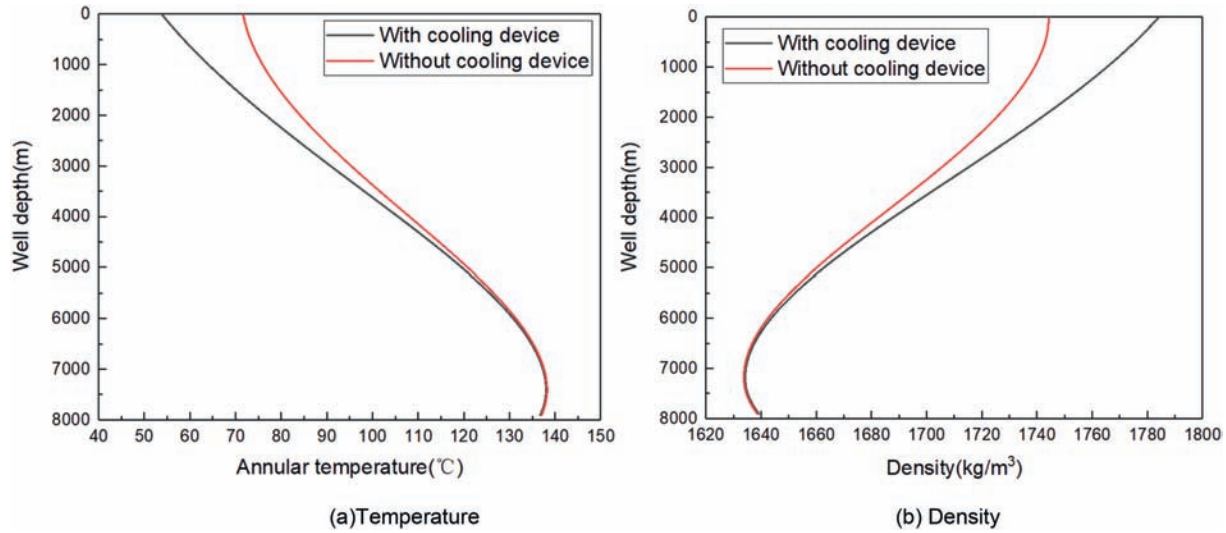


Fig. 9. Annular temperature and density distribution with or without cooling device.

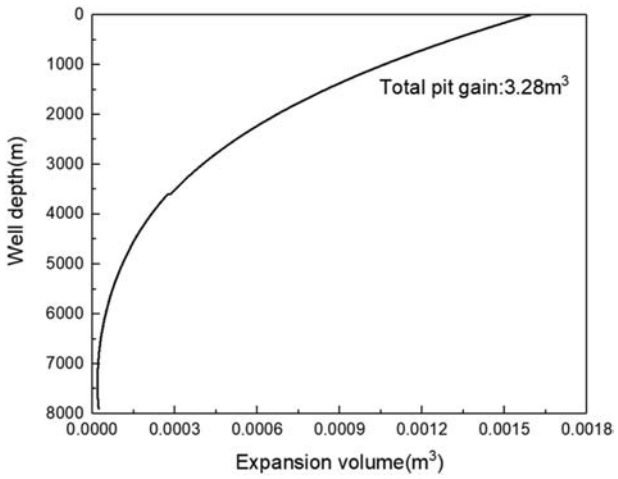


Fig. 10. The expansion volume distribution in wellbore.

formation to the fluid, which increases fluid temperature, increases volume, and decreases density, as shown in Fig. 12b. Thus, the change in drilling fluid volume in the wellbore equals the difference between the volume reduction in the upper section and the volume expansion in the lower section. Because the total volume of fluid in the upper well section is much larger than in the lower section, the total wellbore fluid volume is reduced during tripping operations.

Fig. 13 presents the expansion volume distribution in the wellbore. The cooling device markedly affects the total mud pit volume during tripping operations. When the cooling device is used, the drilling fluid temperature approaches the formation temperature before stopping the pump. Therefore, changes in fluid density and volume are smaller, and the change in mud pit volume is less pronounced. Therefore, to minimize the effect of temperature variation on the total drilling fluid volume, it is recommended to stop the cooling device before POOH.

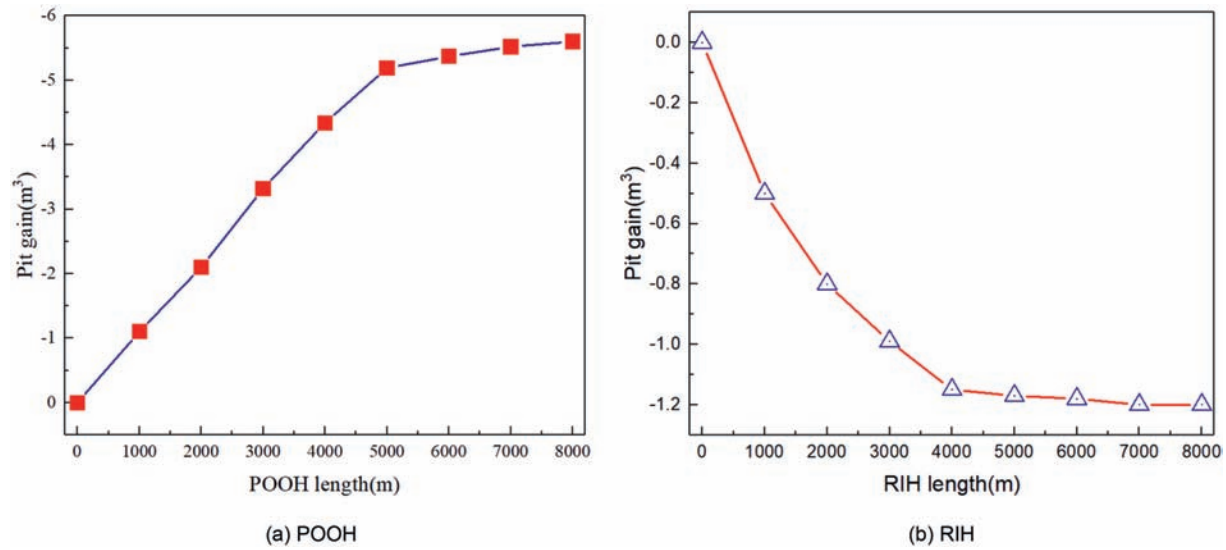


Fig. 11. Measured pit gain variation during POOH and RIH conditions.

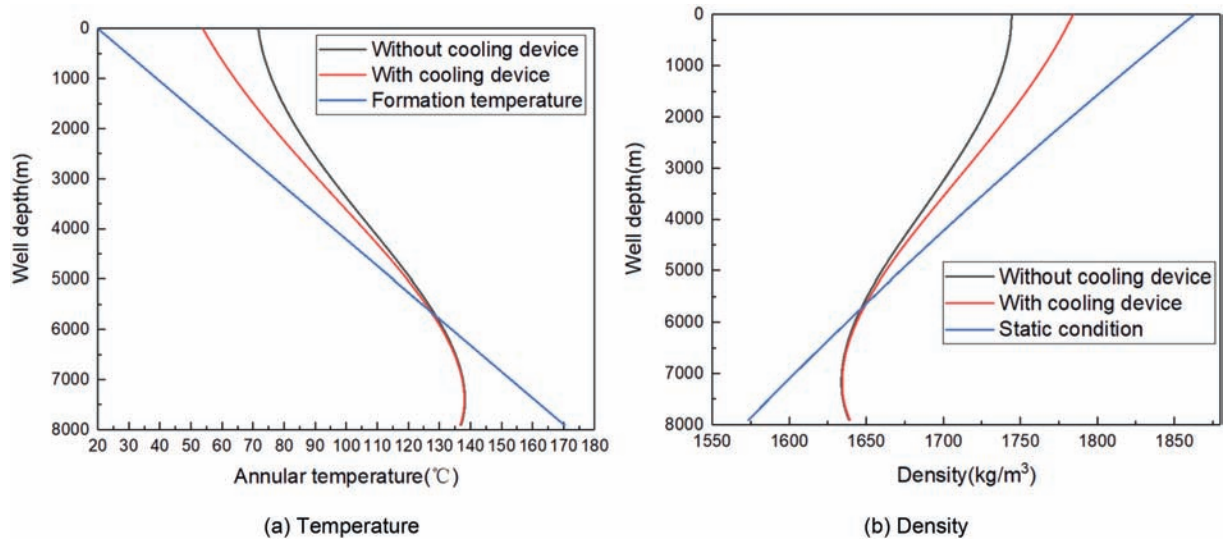


Fig. 12. Annular temperature and density distribution with or without cooling device.

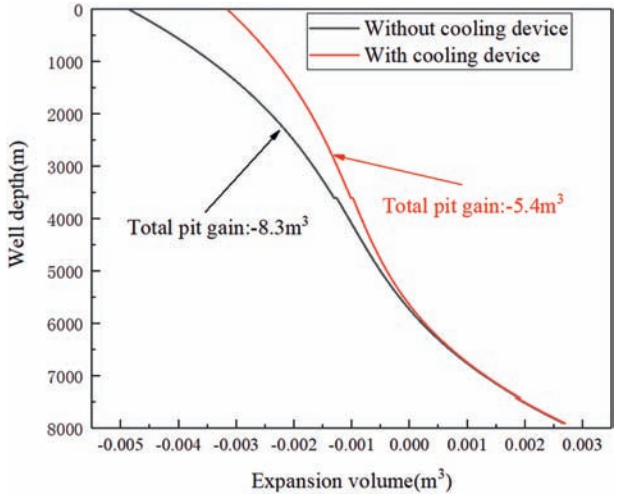


Fig. 13. Expansion volume distribution in the wellbore.

5. Conclusion

(1) This study establishes a mathematical model to predict the expansion of OBD in HTHP wellbores. The model accounts for the variation in rheological properties, thermophysical parameters, and density of OBD with changes in temperature and pressure. The model is solved using discretization and the SOR method.

(2) The rheology and density of OBD at different initial densities are experimentally tested. Binary mathematical models are developed to describe the dependence of OBD density and rheology on temperature and pressure.

(3) The trends in rheological properties of OBD are consistent across different densities. AV and PV decrease and become more stable as temperature increases, and both increase as pressure increases. The density of OBD decreases due to thermal expansion at high temperature and increases due to cold contraction at low temperature. The effect of temperature on OBD density is greater than that of pressure.

(4) The accuracy of the established model is validated using field data inversion from an ultra-deep well. During drilling and tripping, changes in the mud pool volume caused by temperature variation occur gradually, whereas volume changes due to overflow are significantly different because of the slow heat transfer between the formation and the drilling fluid. The model accurately predicts these phenomena. It is recommended that the model presented here be promoted to reduce misjudgment and unnecessary operations by drilling engineers regarding overflow. In addition, it is advised to discontinue the use of the drilling fluid cooling device before POOH to minimize changes in mud pool volume.

CRediT authorship contribution statement

Cai Mingjie: Methodology, Investigation, Funding acquisition, Formal analysis, Data curation, Conceptualization. **Mao Dan:** Formal analysis, Conceptualization. **Li Yuyao:** Validation, Supervision, Software. **He Tingjun:** Resources. **He Mingmin:** Investigation, Conceptualization. **Tan Leichuan:** Methodology.

Declaration of competing interest

The authors declare that there is no conflict of interest regarding the publication of this paper.

Appendix A

(1) Drilling Fluid Inside the Drill String

The energy equation for the drilling fluid inside the drill string is expressed as:

$$U_P^1 = \pi r_1^2 \Delta z (\overline{c\rho T})_P^1 \tag{1}$$

$$U_P^0 = \pi r_1^2 \Delta z (\overline{c\rho T})_P^0 \tag{2}$$

$$Q_n^{0-1} = \pi r_1^2 \Delta t (\overline{c\rho v_i T})_n^{0-1} \tag{3}$$

$$Q_s^{0-1} = \pi r_1^2 \Delta t (\overline{c\rho v_i T})_s^{0-1} \tag{4}$$

$$Q_e^{0-1} = 2\pi r_1 \Delta z \Delta t [\overline{k_e (T_E - T_P)}]^{0-1} \tag{5}$$

$$S_p^{0-1} = \frac{1}{4}\pi r_1 f_s \Delta z \Delta t \left(\overline{\rho v_i^3}\right)^{0-1} \tag{6}$$

Combining Eqs. (1)–(6), the macroscopic energy conservation equation for the drilling fluid inside the drill string is obtained:

$$\begin{aligned}\pi r_1^2 \Delta z \left[(\overline{c\rho T})_P^1 - (\overline{c\rho T})_P^0\right] = {} & \pi r_1^2 \Delta t \left[(\overline{c\rho v_i T})_n^{0-1} - (\overline{c\rho v_i T})_s^{0-1}\right] \\ & + 2\pi r_1 \Delta z \Delta t [\overline{k_e (T_E - T_P)}]^{0-1} \\ & + \frac{1}{4}\pi r_1 f_s \Delta z \Delta t \left(\overline{\rho v_i^3}\right)^{0-1}\end{aligned} \tag{7}$$

(2) Heat Transfer Model for Drill String and Drill Bit

The energy equation for the drill string is expressed as:

$$U_P^0 = \pi \left(r_2^2 - r_1^2\right) \Delta z c_P \rho_P T_p^0 \tag{8}$$

$$U_P^1 = \pi \left(r_2^2 - r_1^2\right) \Delta z c_P \rho_P T_p^1 \tag{9}$$

$$Q_n^{0-1} = \pi \left(r_2^2 - r_1^2\right) \Delta t [\overline{k_P (T_N - T_P)}]^{0-1} \tag{10}$$

$$Q_s^{0-1} = \pi \left(r_2^2 - r_1^2\right) \Delta t [\overline{k_P (T_P - T_S)}]^{0-1} \tag{11}$$

$$Q_e^{0-1} = 2\pi \Delta z \Delta t \left\{ r_2 [\overline{k_e (T_E - T_P)}]^{0-1} - r_1 \left[\overline{k_w (T_p - T_W)}\right]^{0-1} \right\} \tag{12}$$

By substituting Eqs. (8)–(12) into Eq. (2), the macroscopic energy conservation equation for the drill string is derived:

$$\begin{aligned}\pi \left(r_2^2 - r_1^2\right) \Delta z c_P \rho_P \left(T_P^1 - T_P^0\right) = {} & \pi \left(r_2^2 - r_1^2\right) \Delta t [\overline{k_P (T_S + T_N - 2T_P)}]^{0-1} \\ & + 2\pi \Delta z \Delta t \left\{ r_2 [\overline{k_e (T_E - T_P)}]^{0-1} - r_1 \left[\overline{k_w (T_p - T_W)}\right]^{0-1} \right\}\end{aligned} \tag{13}$$

When the control volume represents the drill string, the frictional heat Q_{pf} generated by interaction with the wellbore wall appears on the right-hand side of the equation, mathematically expressed as:

$$\begin{aligned}\pi \left(r_2^2 - r_1^2\right) \Delta z c_P \rho_P \left(T_P^1 - T_P^0\right) = {} & \pi \left(r_2^2 - r_1^2\right) \Delta t [\overline{k_P (T_S + T_N - 2T_P)}]^{0-1} \\ & + 2\pi \Delta z \Delta t \left\{ r_2 [\overline{k_e (T_E - T_P)}]^{0-1} \right. \\ & \left. - r_1 \left[\overline{k_w (T_p - T_W)}\right]^{0-1} \right\} + Q_{pf}\end{aligned} \tag{14}$$

When the control volume represents the drill bit, frictional heat Q_{rg} generated by contact with the formation is also included on the right-hand side, expressed as:

$$\begin{aligned}\pi \left(r_2^2 - r_1^2\right) \Delta z c_P \rho_P \left(T_P^1 - T_P^0\right) = {} & \pi \left(r_2^2 - r_1^2\right) \Delta t [\overline{k_P (T_P - T_N)}]^{0-1} \\ & + 2\pi \Delta z \Delta t \left\{ r_2 [\overline{k_e (T_E - T_P)}]^{0-1} \right. \\ & \left. - r_1 \left[\overline{k_w (T_p - T_W)}\right]^{0-1} \right\} + Q_{rg}\end{aligned} \tag{15}$$

(3) Annular Drilling Fluid

The energy equation for the drilling fluid in the annulus is expressed as:

$$U_p^0 = \pi \left(r_3^2 - r_2^2\right) \Delta z (\overline{c\rho T})_P^0 \tag{16}$$

$$U_p^1 = \pi \left(r_3^2 - r_2^2\right) \Delta z (\overline{c\rho T})_P^1 \tag{17}$$

$$Q_s^{0-1} = \pi \left(r_3^2 - r_2^2\right) \Delta t (\overline{c\rho v_a T})_s^{0-1} \tag{18}$$

$$Q_n^{0-1} = \pi \left(r_3^2 - r_2^2\right) \Delta t (\overline{c\rho v_a T})_n^{0-1} \tag{19}$$

$$Q_e^{0-1} = 2\pi \Delta z \Delta t \left\{ r_3 [\overline{k_e (T_E - T_P)}]^{0-1} - r_2 [\overline{k_w (T_P - T_W)}]^{0-1} \right\} \tag{20}$$

$$S_p^{0-1} = \frac{1}{4}\pi (r_2 + r_3) f_s \Delta z \Delta t \left(\overline{\rho v_a^3}\right)^{0-1} \tag{21}$$

By substituting Eqs. (16)–(21) into Eq. (2), the macroscopic energy conservation equation for the drilling fluid in the annulus is obtained:

$$\begin{aligned}\pi \left(r_3^2 - r_2^2\right) \Delta z \left[(\overline{c\rho T})_P^1 - (\overline{c\rho T})_P^0\right] = {} & \pi \left(r_3^2 - r_2^2\right) \Delta t \left[(\overline{c\rho v_a T})_s^{0-1} \right. \\ & \left. - (\overline{c\rho v_a T})_n^{0-1}\right] \\ & + 2\pi \Delta z \Delta t \left\{ r_3 [\overline{k_e (T_E - T_P)}]^{0-1} \right. \\ & \left. - r_2 [\overline{k_w (T_P - T_W)}]^{0-1} \right\} \\ & + \frac{1}{4}\pi (r_2 + r_3) f_s \Delta z \Delta t \left(\overline{\rho v_a^3}\right)^{0-1}\end{aligned} \tag{22}$$

(4) Near-Wellbore Formation

The energy equation for the formation near the wellbore is expressed as:

$$U_p^0 = \pi \left(r_4^2 - r_3^2\right) \Delta z c_P \rho_P T_P^0 \tag{23}$$

$$U_p^1 = \pi \left(r_4^2 - r_3^2\right) \Delta z c_P \rho_P T_P^1 \tag{24}$$

$$Q_s^{0-1} = \pi \left(r_4^2 - r_3^2\right) \Delta t [\overline{k_P (T_S - T_P)}]^{0-1} \tag{25}$$

$$Q_n^{0-1} = \pi \left(r_4^2 - r_3^2\right) \Delta t [\overline{k_P (T_P - T_N)}]^{0-1} \tag{26}$$

$$Q_e^{0-1} = 2\pi\Delta z\Delta t\left\{r_4[\overline{k_e(T_E - T_P)}]^{0-1} - r_3[\overline{k_w(T_p - T_W)}]^{0-1}\right\} \tag{27}$$

By substituting Eqs. (23)–(27) into Eq. (2), the macroscopic energy conservation equation for the near-wellbore formation is obtained:

$$\pi\left(r_4^2 - r_3^2\right)\Delta z c_P\rho_P\left(T_P^1 - T_P^0\right) = \pi\left(r_4^2 - r_3^2\right)\Delta t[\overline{k_P(T_S + T_N - 2T_P)}]^{0-1} + 2\pi\Delta z\Delta t\left\{r_4[\overline{k_e(T_E - T_P)}]^{0-1} - r_3[\overline{k_w(T_p - T_W)}]^{0-1}\right\} \tag{28}$$

Appendix B

The wellbore and formation domains are discretized using grid systems in both axial and radial directions. A second-order upwind scheme is adopted for the convective term, and a fully implicit scheme is applied for the temporal term. By extending the energy equation from a single control volume to the entire spatial domain, the discretized temperature model for the wellbore and formation is obtained.

The discretized form of Eq. (7) is:

$$c\rho\pi r_1^2\Delta z\left(T_{i,1}^1 - T_{i,1}^0\right) = c\rho v_1\pi r_1^2\Delta t\left(2T_{i-1,1}^1 - 0.5T_{i-2,1}^1 - 1.5T_{i,1}^1\right) + 2\pi r_1 k_1\Delta z\Delta t\left(T_{i,2}^1 - T_{i,1}^1\right) + \frac{1}{4}\rho v_1^3 f_s\pi r_1\Delta z\Delta t \tag{1}$$

The discretized equation of Eq. (14) is:

$$c\rho\pi\left(r_2^2 - r_1^2\right)\Delta z\left(T_{i,2}^1 - T_{i,2}^0\right) = \pi\left(r_2^2 - r_1^2\right)k_P\Delta t\left(T_{i+1,2}^1 + T_{i-1,2}^1 - 2T_{i,2}^1\right) + 2\pi\Delta z\Delta t\left[r_2k_2\left(T_{i,3}^1 - T_{i,2}^1\right) - r_1k_1\left(T_{i,2}^1 - T_{i,1}^1\right)\right] + Q_{pf} \tag{2}$$

The discretized equation of Eq. (15) is:

$$c\rho\pi\left(r_2^2 - r_1^2\right)\Delta z\left(T_{i,2}^1 - T_{i,2}^0\right) = \pi\left(r_2^2 - r_1^2\right)k_P\Delta t\left(T_{i,2}^1 - T_{i-1,2}^1\right) + 2\pi\Delta z\Delta t\left[r_2k_2\left(T_{i,3}^1 - T_{i,2}^1\right) - r_1k_1\left(T_{i,2}^1 - T_{i,1}^1\right)\right] + Q_{rg} \tag{3}$$

The discretized equation of Eq. (22) is:

$$c\rho\pi\left(r_3^2 - r_2^2\right)\Delta z\left(T_{i,3}^1 - T_{i,3}^0\right) = c\rho v_3\pi\left(r_3^2 - r_2^2\right)\Delta t\left(2T_{i+1,3}^1 - 0.5T_{i+2,3}^1 - 1.5T_{i,3}^1\right) + 2\pi\Delta z\Delta t\left[r_3k_3\left(T_{i,4}^1 - T_{i,3}^1\right) - r_2k_2\left(T_{i,3}^1 - T_{i,2}^1\right)\right] + \frac{1}{4}\rho v_3^3 f_s\pi(r_2 + r_3)\Delta z\Delta t \tag{4}$$

The discretized equation of Eq. (28) is:

$$c\rho\pi\left(r_j^2 - r_{j-1}^2\right)\Delta z\left(T_{i,j}^1 - T_{i,j}^0\right) = \pi\left(r_j^2 - r_{j-1}^2\right)k_P\Delta t\left(T_{i+1,j}^1 - T_{i-1,j}^1 - 2T_{i,j}^1\right) + 2\pi\Delta z\Delta t\left[r_jk_j\left(T_{i,j+1}^1 - T_{i,j}^1\right) - r_{j-1}k_{j-1}\left(T_{i,j}^1 - T_{i,j-1}^1\right)\right] \tag{5}$$

where $j \geq 4$.

Eqs. (1)–(5) can be unified into the following general form:

$$\alpha_{i,j}T_{i,j}^{t+\Delta t} - \beta_{i,j}T_{i,j}^t = \delta_{i-2,j}T_{i-2,j}^{t+\Delta t} + \varphi_{i-1,j}T_{i-1,j}^{t+\Delta t} + \gamma_{i+1,j}T_{i+1,j}^{t+\Delta t} + \varepsilon_{i+2,j}T_{i+2,j}^{t+\Delta t} + \eta_{i,j-2}T_{i,j-2}^{t+\Delta t} + \theta_{i,j-1}T_{i,j-1}^{t+\Delta t} + \sigma_{i,j+1}T_{i,j+1}^{t+\Delta t} + \xi_{i,j+2}T_{i,j+2}^{t+\Delta t} + b_{i,j} \tag{6}$$

The iterative solution is obtained using the Successive Over-Relaxation (SOR) method, expressed as:

$$T_{i,j}^{t+\Delta t(k+1)} = T_{i,j}^{t+\Delta t(k)} + \frac{\omega}{\alpha_{i,j}}\begin{bmatrix}\beta_{i,j}T_{i,j}^t + \delta_{i-2,j}T_{i-2,j}^{t+\Delta t(k+1)} + \varphi_{i-1,j}T_{i-1,j}^{t+\Delta t(k+1)} + \gamma_{i+1,j}T_{i+1,j}^{t+\Delta t(k)} \\ + \varepsilon_{i+2,j}T_{i+2,j}^{t+\Delta t(k)} + \eta_{i,j-2}T_{i,j-2}^{t+\Delta t(k+1)} + \theta_{i,j-1}T_{i,j-1}^{t+\Delta t(k+1)} \\ \sigma_{i,j+1}T_{i,j+1}^{t+\Delta t(k)} + \xi_{i,j+2}T_{i,j+2}^{t+\Delta t(k)} + b_{i,j} - \alpha_{i,j}T_{i,j}^{t+\Delta t(k)}\end{bmatrix} \tag{7}$$

References

Cai, M., Mao, L., Xing, X., Zhang, H., Li, J., 2022. Analysis on the nonlinear lateral vibration of drillstring in curved wells with beam finite element. Commun. Nonlinear Sci. Numer. Simul. 104, 106065.

Ding, L., Chen, W., Han, C., Geng, H., Zhang, Q., 2023. Research on a typical casing failure during drilling of cement plugs in ultradeep wells. SPE J. https://doi.org/10.2118/215837-pa.

Fan, W., Shi, W., Tang, L., Chen, S., Zhou, X., Huang, D., Lai, N., 2024. Temperature-responsive Nano-SiO2 composite for improving shale stability in oil-based drilling fluids. Energy. Fuels. 38 (9), 13. https://doi.org/10.1021/acs.energyfuels.3c04295.

James, R.W., Navestad, P., Schei, T., Geddes, T.A., Nelson, G., Webster, D., 2000. Improving the working environment and drilling economics through better understanding of oil-based drilling fluid chemistry. SPE Drill. Complet. 15 (4), 254–260. https://doi.org/10.2118/67835-pa.

Jiang, G.C., Shi, H., He, Y.B., 2022. The biodiesel-based flat-rheology drilling fluid system. Petrol. Explor. Dev. 49 (1), 200–210.

Kabir, S., Hasan, A.R., Kouba, G.E., Ameen, M.M., 1996. Determining circulating fluid temperature in drilling, workover, and well control operations. SPE Drill. Complet. 11 (2), 74–79. https://doi.org/10.2118/24581-PA.

Liu, J.L., Li, J., He, J.T., Yang, H.W., Liu, G.H., Li, H., 2024. A segmented prediction method for fluid density and rheology during managed pressure cementing injection stage. Petr. Drill. Tech. 52 (1), 45–53. https://doi.org/10.11911/syztjs.2024005.

Mahmoud, A., Gajbhiye, R., Elkatatny, S., 2025. Enhanced performance of oil-based drilling fluids under HPHT conditions using an organophilic phyllosilicate. Sci. Rep. 15 (1). https://doi.org/10.1038/s41598-025-05864-7.

Malachosky, E., Shannon, B.E., Jackson, J.E., Aubert, W.G., 1991. Offshore Disposal of oil-based drilling-fluid waste: an environmentally acceptable solution. SPE Drill. Complet. 8 (4), 283–287. https://doi.org/10.2118/23373-PA.

Mao, L.J., Wei, C.J., Jia, H., 2023. Prediction model of drilling wellbore temperature considering bit heat generation and variation of mud thermophysical parameters. Energy 284, 129341.

Mao, L., Liu, Y., Wei, C., Chen, X., Yang, S., 2024. Temperature prediction of geothermal drilling considering the drilling fluid thermophysical parameters. Renew. Energy 237. https://doi.org/10.1016/j.renene.2024.121489.

Mcmordie, W.C., Bland, R.G., Hauser, J.M., 1982. Effect of temperature and pressure on the density of drilling fluids. SPE 11114. https://doi.org/10.2118/11114-MS.

Santoyo, E., Santoyo-Gutiérrez, S., García-Gutierrez, A., Espinosa-Paredes, G., Moya, S., 2001. Rheological property measurement of drilling fluids used in geothermal wells. Appl. Therm. Eng. 21 (3), 283–302.

Wang, C., Liu, H., Yu, G., Yi, C., Liu, X., Huang, P., 2024. Wellbore-heat-transfer-model-based optimization and control for cooling downhole drilling fluid. Pet. Sci. 21 (3). https://doi.org/10.1016/j.petsci.2023.11.025.

Xiao, D., Chen, L., Xu, X., Tang, G., Hu, Y., Guo, B., Liu, M., Yuan, C., Li, G., 2024. Coupling model of wellbore heat transfer and cuttings bed height during horizontal well drilling. Phys. Fluids 36 (9), 097163. https://doi.org/10.1063/5.0222401.

Xie, C., Yang, L., Jiang, G., Ao, T., Cao, F., He, Y., Nie, Q., 2021. Rheological characteristics of oil base drilling fluids and its mathematical model under coupled hthp conditions. Drill. Fluid Complet. Fluid 38 (5), 568–575. https://doi.org/10.12358/j.issn.1001-5620.2021.05.005.

Yu, Y., Wang, X.R., Ke, K., Wang, D., Yu, X., Gao, Y., 2021. Prediction model and distribution law study of temperature and pressure of the wellbore in drilling in Arctic region. Petr. Drill. Tech. 49 (3), 11–20. https://doi.org/10.11911/syztjs.2021047.

Zhao, S.Y., Yan, J.N., Shu, Y., Li, H.K., Li, L., Ding, T.W., 2009. Prediction model for rheological parameters of oil-based drilling fluids at high temperature and high pressure. Acta Pet. Sin. 30 (4), 603–606. https://doi.org/10.7623/syxb200904023.

Zhong, H.Y., Shen, G.C., Qiu, Z.S., Lin, Y.X., Fan, L.J., Xing, X.D., Li, J., 2019. Minimizing the HTHP filtration loss of oil-based drilling fluid with swellable polymer microspheres. J. Petrol. Sci. Eng. 172, 411–424. https://doi.org/10.1016/j.petrol.2018.09.074.

Zhou, J., Kang, Y., Xu, C., Ma, C., 2025. Innovative method to select optimal Plugging materials for preventing loss circulation in deep fractured reservoirs using machine learning. SPE J. 30 (1), 17. https://doi.org/10.2118/223950-PA.